Supplement

Development of 13.5-meter-tall Vibration Isolation System for the Main Mirrors in KAGRA

Koki Okutomi

Chapter 2

Vibration isolation system

2.6 Damping

Mechanical filters can isolate suspended masses from the seismic motion in high frequency region. Meanwhile, they carry the vibration directly to the masses at low frequencies or rather amplify the magnitude of the masses' fluctuation at the resonant frequencies. The amplification at these mechanical resonances often takes place out of the observational band, and thus has no immediate harm to the sensitivity of the interferometer. However, since the interferometer has to keep its interferred light in a specific condition with a narrow-ranged control, it cannot be operated with the largely-swinging mirrors with which the control can no longer survive. Therefore, the effective fluctuation of the mirrors needs to be reduced regardless of the frequency region.

The effective amplitude of the mirror fluctuation can be evaluated as the root-mean-square (RMS) amplitude. The RMS amplitude of a time-varying physical value $x(t)$ is defined as follows,

$$x_{\mathrm{RMS}} \equiv \sqrt{\int_a^b S_x(\omega)\,\mathrm{d}\omega}\ , \tag{2.1}$$

where $S_x(\omega)$ is the power spectral density of x. The interval of the integral is commonly set to $0 \sim \infty$, or sometimes set to a frequency region of interest. The RMS amplitude of the seismic motion is typically in the order of microns at the ground surface and submicrons for underground. In the case of suspension systems which often has mechanical resonances below 1 Hz, the main contribution to the RMS amplitude comes from the peaks in low frequency band ($\lesssim 1$ Hz) where driving disturbances at the resonant peaks are not sufficiently attenuated.

For the reasons above, implementation of damping mechanism is necessary for the suspension systems in gravitational wave telescopes. Damping in a physical system means introducing dissipation processes into the system by intention to produce resistive force on the

oscillating object. We install the damping mechanism on the suspension system in order not only to reduce the RMS amplitude but also to increase the robustness against the unwanted sudden disturbances such as earthquakes and falsely-injected actuation forces. If large amplitude of the mechanical resonances kicked by the immediate disturbance remains for a long time, the interferometer cannot resume its operation which indicates the loss of the duty cycle or duration of its observation. Thus, it is essential to reduce the decay time of the mechanical resonances for the operationability of the interferometer.

There are two ways to implement a damping effect on the suspension system: passive damping and active damping. In the following subsections, the brief explanation of these damping techniques are presented.

2.6.1 Passive damping

Passive damping introduces a viscous element into the system which generates breaking force proportional to the velocity of the oscillator. Letting us consider a mass-spring-damper system illustrated in the left panel of fig. 2.1, the equation of motion of the oscillator is written as below,

$$M\ddot{x} + \gamma(\dot{x} - \dot{x_0}) + k(x - x_0) = 0\,, \tag{2.2}$$

where γ is the damping coefficient. Interpreting this equation in the frequency domain through Fourier transformation, we can derive the transfer function from the ground displacement to the mass displacement such as,

$$H(\omega) \equiv \frac{\tilde{x}(\omega)}{\tilde{x}_0(\omega)} = \frac{1 + 2\mathrm{i}\zeta\dfrac{\omega}{\omega_0}}{1 + 2\mathrm{i}\zeta\dfrac{\omega}{\omega_0} - \left(\dfrac{\omega}{\omega_0}\right)^2}\,, \tag{2.3}$$

where the parameter ζ is called *damping ratio* which is determined by $\zeta = \gamma/2M\omega_0$. The strength of the damping is also sometimes referred to as the quality factor of the resonance which is defined as $Q \equiv 1/2\zeta$.

The vibration isolation ratio of the mass-spring-damper system with varying the strength of the viscous damping denoted as the quality factors Q is plotted in the right panel of fig. 2.1. As the stronger damping is applied on the suspended mass, the height of the resonant peak gets smaller which is approximately equivalent to Q in the case of $Q \gg 1$. On the other hand, the magnitude of the attenuation factor rolls off with the proportionality of f^{-1} in high frequencies above Qf_0, unlike that of the undamped system with f^{-2} roll off. Therefore, the vibration isolation performance of the viscously-damped system becomes degraded in the high frequency region.

The effect of the damping can be seen also in the impulse responses of the mass displacement. Figure 2.2 shows the responses of the viscously-damped system to the external

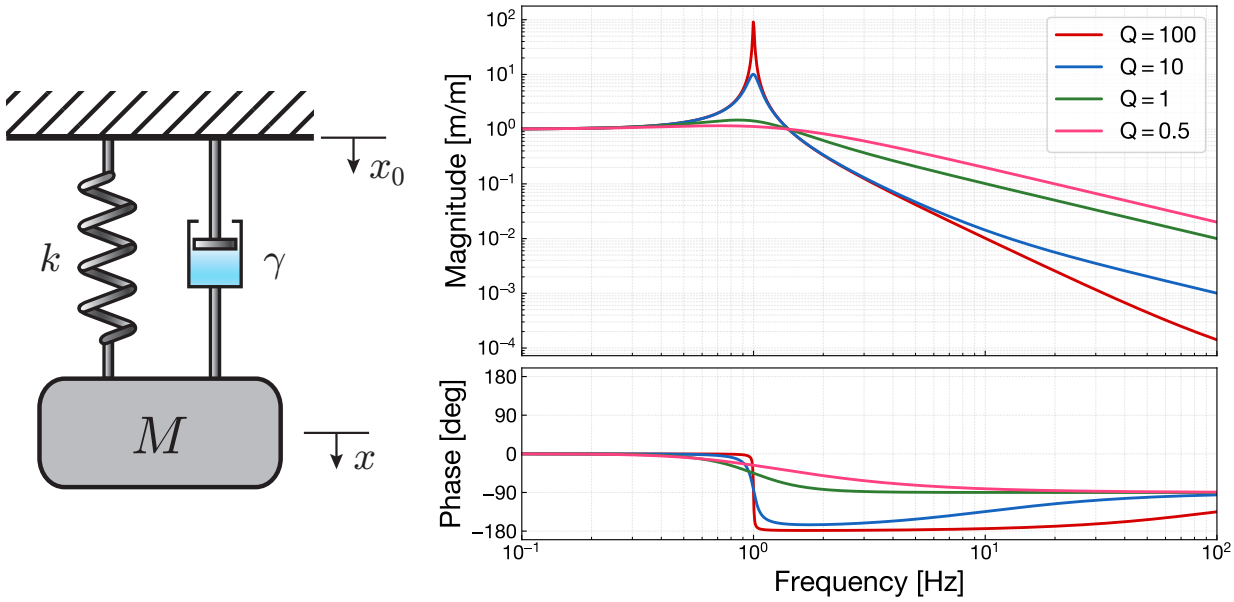

Fig. 2.1. An illustration of the mass-spring-damper system (*left*), and its vibration isolation ratio with various damping strength parametrized by the quality factor Q (*right*). The component of the viscous damping is represented as a dashpot.

impulsive force on the mass, varying the strength of the damping effect. The system with small damping shows sinusoidal waveform with slightly decaying amplitude. As the damping effect getting prominent, the decay of the amplitude quickly becomes in effect. The speed of the decay is characterized by the exponential decay time τ_e in which the oscillation amplitude decreases by a factor of 1/e, which is written as,

$$\tau_e \equiv \frac{1}{\zeta\omega_0} = \frac{2Q}{\omega_0}\,. \tag{2.4}$$

The condition with the damping ratio ζ being one is called *critical damping* where the oscillatory behavior of the impulse response turns to a non-oscillatory transient showing shortest decay time. Then, if the damping ratio increases larger than one, the system gets hard to the external force but meanwhile has longer decay time since the excess of viscosity resists the restoring force to its original position.

The degradation of the vibration isolation performance in the viscously damped system can be mitigated by isolating also the damper with some mechanical filters, as illustrated in fig. 2.3. This technique is called *flexible damping*. Although in the system with flexible damping the tranfer function from the ground motion to the mass displacement has additional resonant peak due to the spring for the damper, the roll off in high frequency region remains f^{-2} proportionality like a system with no damping mechanism.

One simple way to implement the passive damping mechanism is the use of eddy current damper [10]. One unit of the eddy current damper consists of a set of permanent magnets and

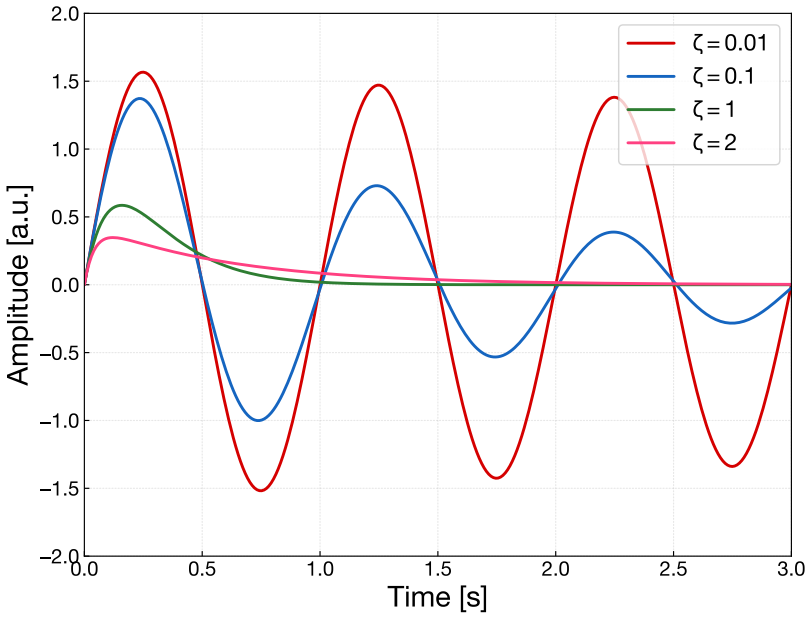

Fig. 2.2. Responses of the viscously damped system with various damping ratios driven by an impulsive force applied on the suspended mass.

a conductive object which are put in facing each other. When the conductive object moves in the magnetic field formed by the permanent magnets, eddy currents are generated inside the conductive object resisting the change of the magnetic field, and thus they produces breaking force of the moving object. The strength of the eddy current damping is formulated as the following relationship,

$$\gamma_{\text{eddy}} = A\sigma B\frac{\partial B}{\partial x}\,, \tag{2.5}$$

where B is the magnetic field of the permanent magnets, σ is the electrical conductivity of the facing object, and A is a geometrical factor determined by the area of the conductor. In qualitative words, stronger magnets and higher conductivity surface can achieve larger damping effect with an eddy current damper. The reason why the eddy current damper is often used in the suspension system among various types of viscous dampers is its vacuum copatibility and the absence of hysteretic noise due to its noncontacting functionality. Nevertheless, the disadvantage of the eddy current damper is the risk of introducing additional magnetic noise onto the test masses which also has permanent magnets for control actuation. This disadvantages can be mitigated by placing the damper apart from the test mass, that is to apply the damper on one of the upper stage.

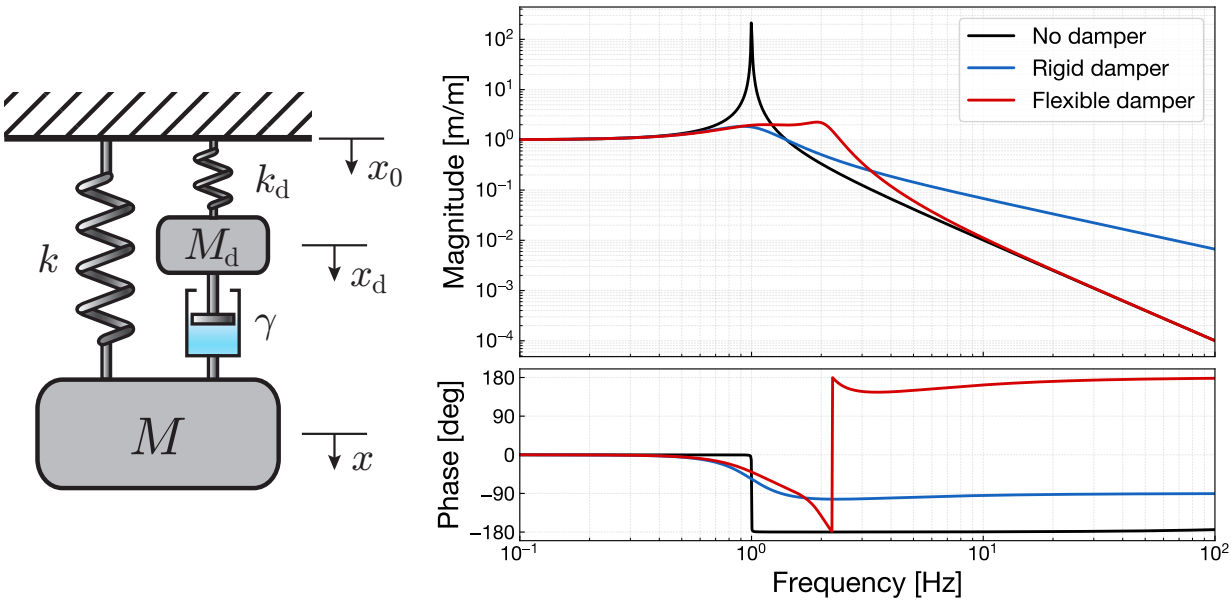
x_0
k_d
k
M_d
x_d
γ
M
x
No damper
Rigid damper
Flexible damper
Magnitude [m/m]
10^{2}
10^{1}
10^{0}
10^{-1}
10^{-2}
10^{-3}
10^{-4}
Phase [deg]
180
90
0
−90
−180
10^{-1}
10^{0}
10^{1}
10^{2}
Frequency [Hz]

Fig. 2.3. test

Chapter 6

Conclusion

Achievement of the requirements

Table 6.1 summarizes the achievements of the requirements for the Type-A suspension. Here the measures evaluated in the performance test of the Type-A tower are only listed. Among the DoFs of our interest, the setup of the Type-A tower cannot yield some meaningful results in the performance in pitch direction since it strongly depends on the multi-wired suspension structure inside the cryogenic payload. In addition, the requirements in the observation phase have to be out of the scope in this experiments due to the similar reasons.

The requirements in the calm-down phase have been satisfied as far as the tower test can validate except for the 1/e modal decay time. Due to the number of eigenmodes the Type-A suspension has and the limitation of the experimental period, the decay time measurement of only the lowest-order eigenmodes is completed. However, the eigenmodes measured in this experiment are the most important ones in terms of the interferometer operation. Although other principal eigenmodes are not evaluated in the measurement, the control simulation presented in chap. 4 predicted that they can be damped sufficiently to achieve the decay time less than 1 minute. The RMS amplitudes required for the calm-down phase are successfully satisfied in the tower stages. Therefore, it is expected that the mirror in the cryogenic payload suspended from the constructed tower can achive the reasonable magnitude.

The performances required in the lock-acquisition phase have been measured and showed sufficiently small RMS values. Note that the ongoing commissioning of the KAGRA inteferometer after this experiments has actually succeeded to lock the arm cavity using the installed Type-A suspension.

Table 6.1. Experimental results of the performance test of the Type-A tower. The measured items only which can make evaluations on the requirements are listed. The yellow highlight indicates that the measured performance doesn't satisfy the requirement.

Calm-down phase			
Item	Measurement	Requirement	Notes
1/e modal decay time	< 44 sec.	< 60 sec.	Yaw 1st–3rd modes
RMS displacement (L)	1.1 μm	< 50 μm	Measured at BF
RMS displacement (T)	1.1 μm	< 100 μm	Measured at BF
RMS displacement (V)	5.3 μm	< 100 μm	Measured at DP
RMS angle (Y)	~ 227 nrad	< 50 μrad	In-loop evaluation at BF
Lock-acquisition phase			
Item	Measurement	Requirement	Notes
RMS velocity (L)	0.73 μm/s	< 240 μm/s	Measured at BF
RMS angle (Y)	~ 227 nrad	< 880 nrad	In-loop evaluation at BF

Citations

The submitted version of the thesis has many references failed to be cited. This chapter patches the sentences in the submitted thesis with approptiate citations by means of copying the corresponding part of the sentences and adding a citation linked to the bibliography in this supplementary document. Those additional citations will be merged into the thesis in the following revisions.

- The concept of gravitational wave appears firstly in the Einstein's letter as an wave solution of the linearized equation of the gravitational field [4, 5]. (Section 1.1, p. 9)
- The first evidence of this orbital energy loss is discovered by Hulse and Taylor in their long-period radio observation of the pulsar binary PSR B1913+16 [6]. (Section 1.2, p. 15)
- The nature of seismic background noise is studied by J. Peterson [9]. (Section 2.1, p. 31)
- **Fig. 2.1.** The New High/Low Noise Model (red curves) with the seismic spectra measured in the world wide network of seismometers [9]. (Section 2.1, p. 32)
- **Fig. 2.2.** Typical power spectrum density of seismic motions at each site of the GW detectors [7]. (Section 2.1, p. 33)
- This saturation is due to a residual momentum transfer from the leg to the payload caused by so-called *center of percussion effect* [12, 2]. (Section 2.4.1, p. 41)
- A getometric anti-spring (GAS) filter is a mechanical oscillator with use of radially converging cantilever blades to obtain a low resonant frequency in vertical direction under heavy load [1, 3]. The quasi-triangular cantilever blades are connected at their vertices with compressing each other. The compression produces repulsive force for the vertical displacement which results in the counter stiffness against the intrinsic stiffness of the cantilever blades. In the situation where the load and compression are tuned appropriately, the GAS filter adequates the low-frequency vertical resonance with typically ~ 0.3 Hz. (Section 2.4.2, p. 44).

- Due to the CoP effect, the seismic attenuation performance of the GAS filter saturates at high frequencies which is typically limited to $\sim 10^{-3}$ [11]. (Section 2.4.1, p.46)
- Detailed discussion on the active isolation strategy and instrumentation is available in [8]. (Section 2.5, p. 48)

Bibliography

[1] A. Bertolini et al., *Nucl. Instrum. Methods Phys. Res. A*, **435** (3), pp. 475–483, (1999). "Seismic noise filters, vertical resonance frequency reduction with geometric anti-springs: A feasibility study", (cited on p. 11).

[2] M. Blom, *phdthesis*, Vrije Universiteit, (2015). "Seismic attenuation for Advanced Virgo Vibration isolation for the external injection bench", (cited on p. 11).

[3] G. Cella et al., *Nucl. Instrum. Methods Phys. Res. A*, **540** (2-3), pp. 502–519, (2005). "Monolithic geometric anti-spring blades", (cited on p. 11).

[4] A. Einstein, *Sitzungsberichte der Königlich Preußischen Akademie der Wissenschaften (Berlin)*, **1**, pp. 688–696, (1916). "Näherungsweise Integration der Feldgleichungen der Gravitation", (cited on p. 11).

[5] A. Einstein, *Sitzungsberichte der Königlich Preußischen Akademie der Wissenschaften (Berlin)*, **1**, pp. 154–167, (1918). "Über Gravitationswellen", (cited on p. 11).

[6] R. A. Hulse and J. H. Taylor, *Astrophys. J.* **195** (1), pp. L51–L53, (1975). "Discovery of a Pulsar in a Binary System", (cited on p. 11).

[7] LCGT Collaboration, *KAGRA Internal Document*, **JGW-T0400030**, (2009). "LCGT design document ver.3", (cited on p. 11).

[8] F. Matichard et al., *Class. Quantum Grav.* **32** (18), (2015). "Seismic isolation of Advanced LIGO: Review of strategy, instrumentation and performance", (cited on p. 12).

[9] J. Peterson, *techreport*, **Open-file Report-**, (1993). "OBSERVATIONS AND MODELING OF SEISMIC BACKGROUND NOISE", (cited on p. 11).

[10] H. A. Sodano et al., *J. Vib. Acoust.* **128** (3), pp. 294–302, (2006). "Improved Concept and Model of Eddy Current Damper", (cited on p. 5).

[11] A. Stochino et al., *Nucl. Instrum. Methods Phys. Res. A*, **580** (3), pp. 1559–1564, (2007). "Improvement of the seismic noise attenuation performance of the Monolithic Geometric Anti-Spring filters for gravitational wave interferometric detectors", (cited on p. 12).

[12] A. Takamori, *phdthesis*, University of Tokyo, (2002). “Low frequency seismic isolation for gravitational wave detectors”, (cited on p. 11).